Characterization of high quality InN grown on production-style plasma assisted molecular beam epitaxy system

I. Gherasoiu,[a] M. O'Steen, T. Bird, and D. Gotthold
Veeco Instruments Inc., MBE Operations, 4900 Constellation Drive, St. Paul, Minnesota 55127

A. Chandolu, D. Y. Song, S. X. Xu, M. Holtz, and S. A. Nikishin
Nano Tech Center, Texas Tech University, Lubbock, Texas 79409

W. J. Schaff
Department of Electrical and Computer Engineering, Cornell University, Ithaca, New York 14583

(Received 13 December 2007; accepted 25 February 2008; published 4 April 2008)

In this work, the authors report step-flow growth mode of InN on [0001] oriented GaN templates, using a production-style molecular beam epitaxy system, Veeco GEN200®, equipped with a plasma source. Using adaptive growth conditions, they have obtained a surface morphology that exhibits the step-flow features. The root mean squared roughness over an area of 5×5 μm^2 is 1.4 nm with monolayer height terrace steps (0.281 nm), based on atomic force microscopy. It has been found that the presence of In droplets leads to defective surface morphology. From x-ray diffraction, they estimate edge and screw dislocation densities. The former is dominant over the latter. Micro-Raman spectra reveal narrow E_2^2 phonon lines consistent with excellent crystalline quality of the epitaxial layers. The Hall mobility of 1 μm thick InN layers, grown in step-flow mode, is slightly higher than 1400 $cm^2/V\,s$, while for other growth conditions yielding a smooth surface with no well-defined steps, mobility as high as 1904 $cm^2/V\,s$ at room temperature has been measured. The samples exhibit high intensity photoluminescence (PL) with a corresponding band edge that shifts with free carrier concentration. For the lowest carrier concentration of 5.6×10^{17} cm^{-3}, they observe PL emission at ~0.64 eV. © *2008 American Vacuum Society.* [DOI: 10.1116/1.2899412]

I. INTRODUCTION

The energy gap of InN has been a subject of controversy due to the large range of values reported for the fundamental gap. Recent work has interpreted the range of values based on free carrier concentration and the consequent filing of the conduction band.[1] Alternative explanations for the variations reported in literature rely on the formation of In_2O_3 with larger band gaps in layers contaminated by oxygen[2] and on the presence of In clusters in InN epilayers.[3] The narrow band gap at room temperature of InN [around 0.7 eV (Refs. 4–6)] promises new applications well into the infrared range, at wavelengths suitable for optical communications. Alloys of InN with Ga and Al may also be used in applications for high efficiency solar cells[7,8] and terahertz emitters.[9]

Despite this potential, the difficulty of obtaining high quality InN, with atomically flat surfaces and good electronic properties, remains a main challenge for future device development. In order to fully explore the applications of InN, further studies focusing on crystal growth are needed to understand the relation between the growth conditions and electronic properties.

In this article, InN growth is carried out using a production-style, molecular beam epitaxy system equipped with radio-frequency (rf) plasma source. We investigate the properties of two sets of InN samples obtained using two different growth approaches that were monitored based on *in situ* reflection high-energy electron diffraction (RHEED) images. The first set (A) is produced using fixed III–V flux ratios during the entire growth period. The second set (B) is obtained using an adaptive method in which III–V flux ratios are controlled to preserve a consistent two-dimensional (2D) growth mode during the entire growth period. High quality InN and In-rich InGaN can be obtained only in a narrow range of growth parameters.[10,11] Here we demonstrate high quality InN using a large capacity plasma assisted molecular beam epitaxy (PAMBE) system suitable for wide scale production of devices based on InN and related alloys.

II. EXPERIMENTAL DETAILS

Growth experiments were performed on 50 mm diameter, on-axis [0001] oriented GaN templates, grown on sapphire using metal-organic chemical vapor deposition (MOCVD). A Veeco GEN200® MBE system, adapted for autonomous operation, was used for the plasma assisted growth of GaN and InN layers at the Veeco Process Integration Center. GaN buffers followed by InN were grown without removing the wafers from the growth chamber in a multiwafer platen capable of holding 13 substrates. High purity N_2 flow has been used with a Veeco UNI-Bulb® rf plasma source to deliver the active nitrogen to the growth surface. Gallium (5000 g capacity) and indium (5000 g capacity) SUMO® effusion cells were used to generate Ga and In fluxes, respectively. The chamber pressure during the growth was maintained in the low to mid-10^{-5} Torr range. A large-area heater ensured temperature uniformity during the growth at high and low temperatures. The RHEED parameters were monitored *in*

[a]Electronic mail: igherasoiu@veeco.com and igheraso@yahoo.com

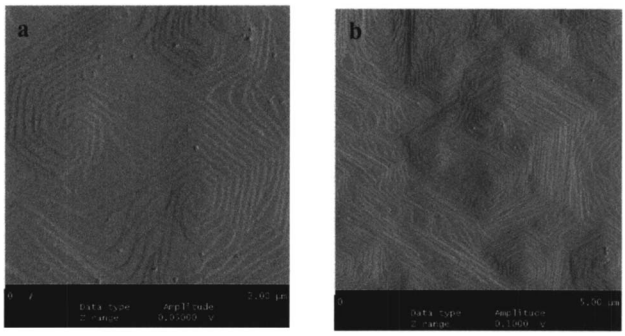

FIG. 1. Surface morphology of GaN buffer layer determined by AFM. (a) Scanned area of 2×2 μm^2 with a rms roughness of 0.88 nm; (b) 5×5 μm^2 with a rms roughness of 2.6 nm.

situ during the growth using kSA 400 RHEED analysis system (*k*-Space Associates, Inc.) and a RHEED electron gun system (Staib Instruments Inc.).

Samples were characterized postgrowth in order to examine the structural, electrical, and optical properties. The surface and bulk properties were studied using atomic force microscopy (AFM), scanning electron microscopy (SEM), and high-resolution x-ray diffraction (XRD). Carrier transport characteristics were obtained using Hall measurements at room temperature and 80 K. Raman spectroscopy at room temperature and 20 K was performed to investigate sample quality, and the optical characteristics of the samples were examined using room temperature photoluminescence (PL). The polarity of GaN template or that of the InN layer has not been investigated directly. However, similar templates have been used for ammonia-based growth of GaN. At the end of the MBE growth with NH_3, GaN surface exhibited (2×2) reconstruction characteristic for Ga polar GaN layers.[12] Therefore, we would support the idea that the MOCVD GaN templates used in this study are Ga polar and furthermore that InN grown on these templates is In polar.

For each experiment, GaN templates have been overgrown at 720 °C with a 300 nm thick GaN buffer deposited by PAMBE. To ensure the good quality of the subsequent layers, the GaN buffers were grown under conditions known to produce step-flow growth and droplet-free surfaces.[13,14] Surface morphology of these GaN buffers was examined by AFM measurements on separate samples, as presented in Fig. 1.

Following the growth of GaN buffer, the temperature was decreased (457–487 °C) and InN growth initiated. Layers of 1 μm thick InN were deposited at a growth rate of 0.25 μm/h using a N_2 flow of 8 SCCM (SCCM denotes cubic centimeter per minute at STP) and a rf power of 600 W, under slightly In-rich conditions.[15,16]

III. RESULTS AND DISCUSSION

The parameters of two sets of samples are summarized in Table I. For group A, the growth conditions that have been established at the beginning of the growth were maintained unchanged for the entire deposition period. For this group, the RHEED pattern at the beginning of the growth exhibited the characteristics of pure two-dimensional (2D) growth mode. At the end of the growth period (4 h), all but one sample in this group underwent a transition to three-dimensional (3D) growth to various degrees. Early transition to 3D growth mode resulted in rough surfaces, while transition to 3D later in the growth cycle resulted in smoother surfaces. In the case of A4 sample, smooth characteristics were obtained without resolved atomic steps. This 2D to 3D growth evolution is indicative of small deviations from the optimal III–V ratio on the growth surface. We suggest that excess nitrogen depletes the In adlayer leading to the onset of 3D growth. In contrast, indium excess leads to a thicker adlayer and thereby impeding active nitrogen diffusion to the growth surface, resulting in a diminished growth rate.

For group B, an adaptive deposition method has been used, in which we modify the growth parameters based on the monitoring of the features of the RHEED pattern. In this case, the III-N ratio on the growth surface is continuously adjusted within a narrow range and a streaky RHEED pattern indicative of a two-dimensional surface is maintained throughout the growth period. The surface temperature and the V/III beam equivalent pressure ratio are summarized for all samples in Table II. The resulting InN layer possesses a

TABLE I. Summary of the morphological, structural, and electrical characterizations for the two growth methods.

Sample	2×2 μm^2 RMS (nm)	Dislocations: Screw (cm^{-2}) $\times10^9$ GaN	Dislocations: Screw (cm^{-2}) $\times10^9$ InN	Dislocations: Edge (cm^{-2}) $\times10^{10}$ GaN	Dislocations: Edge (cm^{-2}) $\times10^{10}$ InN	RT mobility ($cm^2/V\,s$)	n_v ($\times10^{18}$)	Morphology
A1	10.2	3.1	3.5	2.8	10.2	1316	0.98	Rough
A2	>20.0	2.7	3.2	2.8	6.9	1024	0.59	Very rough
A3	3.5	2.3	2.4	2.7	9.4	1481	1.36	Grainy
A4	2.9	2.2	6.7	2.6	6.1	1152	4.18	Smooth, no steps
B1	0.9	2.7	3.5	2.5	8.7	1422	3.17	Step-flow growth
B2	1.7	2.1	2.5	2.7	10.0	1904	1.94	Smooth, no steps
B3	0.7	2.6	2.7	2.7	13.8	1404	3.2	Step-flow growth
B4	1.0	2.2	2.3	2.7	13.5	1800	2.0	Disturbed step-flow growth

TABLE II. Summary of the main growth conditions for the two sample groups.

Sample	Surface Temperature (°C)	V/III BEP ratio
A1	487	118
A2	487	202
A3	474	118
A4	457	108
B1	487	108
B2	487	108
B3	487	108
B4	487	108

smooth surface with approximately one atomic layer step height, characteristic of the step-flow growth mode. The presence of threading dislocations at the surface of MOCVD GaN templates is a common feature and it is known to induce hillock formation through a step motion mechanism based on the terrace-step-kink model described originally by Burton *et al.*[16] We have based our assessment of step-flow growth mode on the lack of observable island nucleation on the terraces between steps that would be indicative of the layer-by-layer growth mode. It is also true that such observation may be considered only indirect evidence of step-flow growth as opposed to more direct evidence that could be obtained from the monitoring of RHEED intensity. The AFM results, presented in Fig. 2, have rms roughnesses of 0.7 nm for the 2×2 μm^2 scan and 1.4 nm for the 5×5 μm^2 scan. As shown in Fig. 2(c), step height measurements of the terrace edges indicate a height of 0.28 nm. This height corresponds to one monolayer of InN, representing half of *c*-axis lattice constant of InN.

These surface characteristics are similar to the recently reported step-flow growth of In-polar InN by MBE.[17] The InN layer exhibits, on average, a reduced number of small and shallow growth pits (less than 20 in 100 μm^2 area) while relatively large areas are free of pits. Indium droplets with a diameter $\leqslant 15$ μm were observed on the surfaces of all samples following the growth. Controlling the In amount on the surface and understanding the mechanism of In droplet formation are required to ensure InN layers with the high quality surfaces.

Ideally, the formation of InN epitaxial surface takes place under a uniform adlayer of In with a thickness in the range of a few monolayers, similar to the phenomenology described for PAMBE of GaN.[14,18] The vapor-liquid-solid (VLS) growth mode is the mechanism that allows active nitrogen to permeate In adlayer, diffuse along the surface, and ultimately to incorporate in the epitaxial layer. Even under ideal conditions, it is not possible to entirely avoid the formation of In droplets. This is because In cannot be completely evaporated at the low growth temperature and droplets form on the surface during the cooling stage. Chemical removal of indium using HCl should reveal a smooth InN surface, free of discontinuities.

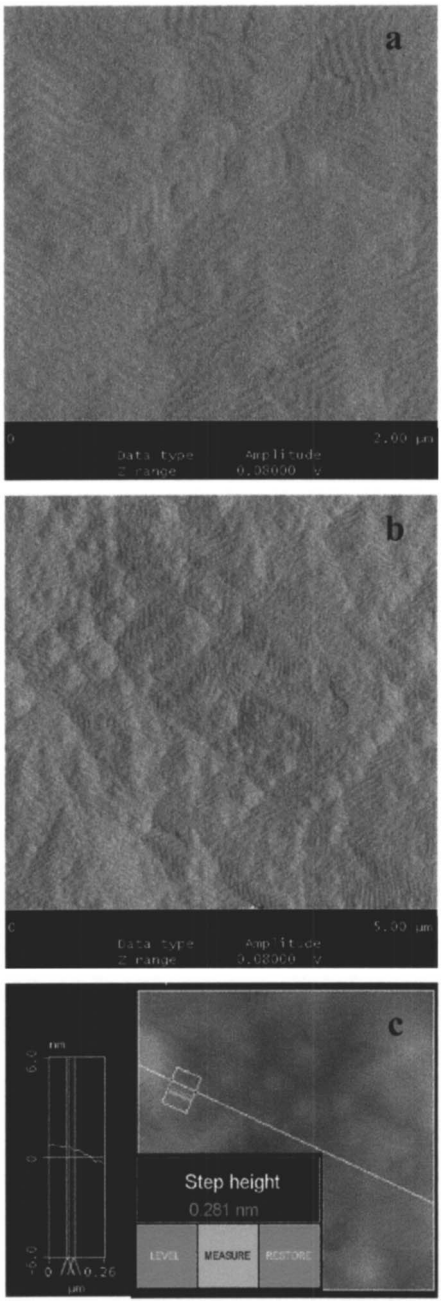

FIG. 2. Surface morphology of InN film showing step-flow characteristics. (a) Scan area of 2×2 μm^2 with a rms roughness of 0.7 nm. (b) Scan area of 5×5 μm^2 with a rms roughness of 1.4 nm. (c) Measurement of step height indicating monolayer terrace steps.

However, under less than ideal conditions, In droplets may form during the early stages of the InN growth. The growth conditions under a droplet differ from those under the uniform In layer due to the geometrical factors. Surface diffusion of the active nitrogen on uniform, quasiplanar In adlayers, followed by bulk liquid diffusion, has no preferential direction. Therefore, the epitaxial layer underneath will exhibit uniform thickness due to the uniform flux of active

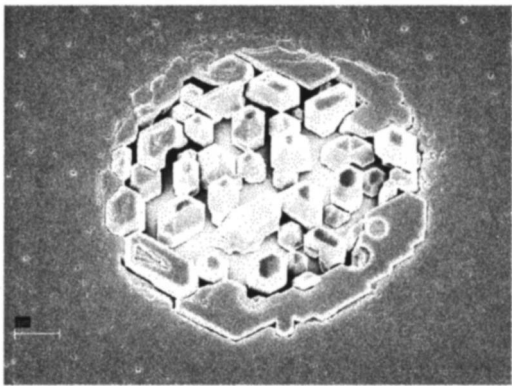

FIG. 3. Defective area formed underneath an In droplet.

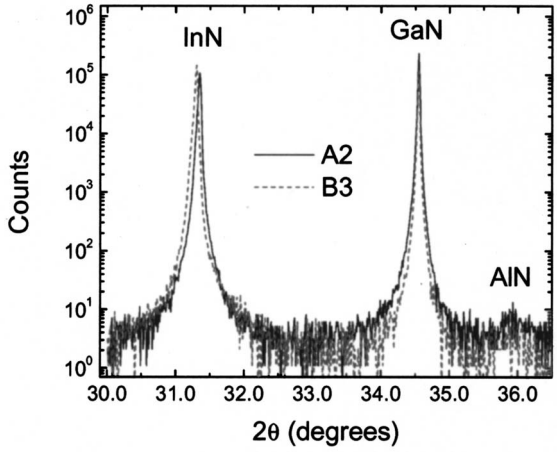

FIG. 4. X-ray diffraction of InN grown on GaN/sapphire templates, $\omega/2\theta$ scan of (0002) planes.

nitrogen supplied over a large area. However, we conjecture that within the In droplet, the average length of the bulk diffusion may be shorter than the radius of the droplet. As a consequence, a large fraction of active nitrogen will not be able to reach the growth interface. This nitrogen would either recombine to form neutral molecular nitrogen or, more likely, would form InN slabs in suspension. Consequently, the solid-liquid interface underneath the droplet would be depleted of nitrogen species and the growth will be retarded, resulting in a defective area with nonuniform appearance. Upon the chemical removal of indium droplets, substantially different crystal formation can be observed. A representative SEM picture in Fig. 3 shows the approximately circular shape of the macroscopic defects. The diameter of the defective area is consistent with that of the pre-etch In droplet. Toward the center of the droplet region, we see sparse coverage by small InN crystals. Shapes are clearly reminiscent of hexagonal symmetry. Lateral growth of these crystals is impeded by factors such as unequal growth rates associated with different crystalline planes, limited nitrogen transport to the side facets of these crystals (shadowing effect) when compared with the crystal plane on top, etc.

As we move toward the perimeter of this region, the coverage increases and ultimately the crystal merges with the surrounding uniform region having planar InN coverage. Similar phenomenology has been reported previously for the formation of macroscopic defects on (100) GaAs layers grown by MBE.[19] It should be noted that once formed In droplets are likely to be sustained throughout the growth. Therefore, the In delivery rate at the epitaxial surface needs to be carefully optimized and maintained along the growth period.

Crystal quality has been investigated by XRD, using both symmetric and asymmetric diffraction arrangements. Threading dislocation densities with screw and edge components have been thus estimated. Edge dislocation density was estimated based on both asymmetric and skew symmetric XRD measurements. Crystal lattice parameters and stress have been also determined through the XRD measurements for both GaN and InN layers. The c and a lattice parameters were obtained using diffraction angles of symmetric (0002) and asymmetric $(11\bar{2}4)$ reflections, respectively.[20,21] The (0002) ω-scan and $2\theta/\omega$-scan measurements have been performed on both MOCVD GaN templates and InN layers. For the GaN templates, (0002) ω-scan measurements showed full width at half maximum (FWHM) in the range 1150 ± 20 arc sec, while InN grown on these templates exhibits slightly larger FWHM values. Representative 2θ-ω scans for the A and B sample groups are presented in Fig. 4. Clearly seen are narrow diffraction lines from the GaN template and the overgrown InN layer.

The deviation seen in InN (0002) diffraction angle, Fig. 4, is due to the differences in the amount of stress in the two samples. Comparing the relaxed[22] and measured lattice parameters, the compressive biaxial stress was estimated to range from 0.18 to 0.48 GPa in the samples studied here using published elastic moduli.[23] Threading dislocations (screw and edge) are the dominant defects present in InN epitaxial layers.[24] Screw dislocation densities in the range of $(2-7) \times 10^9$ cm^{-2} were calculated from the FWHM of (0002) reflection.[25] The dependences of FWHM of $(10\bar{1}1)$, $(10\bar{1}2)$, $(10\bar{1}3)$, $(10\bar{1}5)$, and $(30\bar{3}2)$ Φ and ω scans on the inclination angle ϕ were used to estimate the edge dislocation density. Figure 5 summarizes these measurements for a typical InN epilayer. The FWHM of Φ scans decreases while the FWHM of ω scans increases with the increment of ϕ. Extrapolating these dependences to $\phi = 90°$, where the reflection plane is perpendicular to the sample surface, we obtain FWHM for this plane.[26] Using this approach, we obtain edge dislocation densities in the range of $(6-13) \times 10^{10}$ cm^{-2}. These values are typical for MBE grown InN samples.[23]

Screw and edge dislocation densities obtained from the x-ray measurements were compared between the GaN template layer and the InN. Screw dislocation densities of the InN layers exhibit a very close correlation with that of their respective templates being consistently higher by less than 30%. However, for both sets of samples studied, we observe no correlation between InN and GaN edge dislocation densities. For these dislocations, the densities associated with

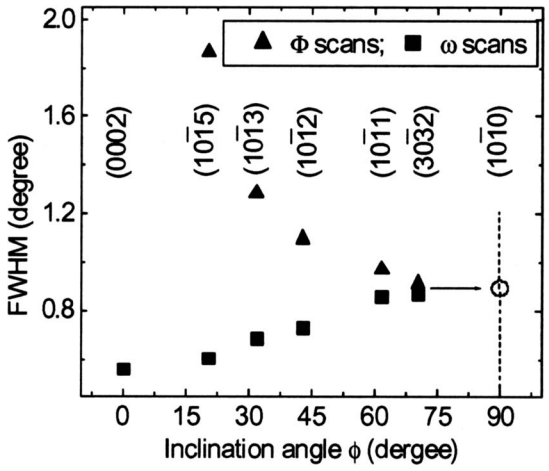

FIG. 5. Linewidth dependence of Φ scans (triangles) and ω scans (squares) for (*hkil*) reflections as a function of inclination angle ϕ of lattice planes with respect to the sample surface for a typical InN epitaxial layer grown on GaN template.

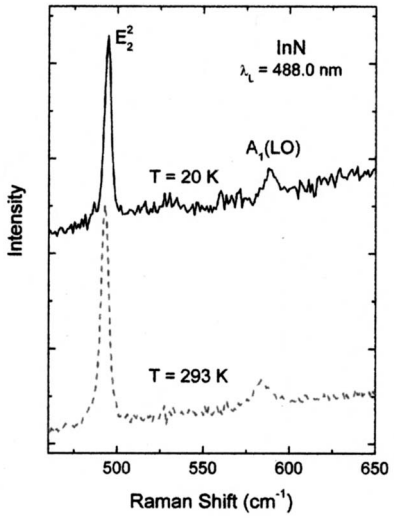

FIG. 6. Raman spectra of InN at 20 K and ambient temperature.

InN are a factor of 2–4 higher than for the GaN templates. This could be attributed to the lattice mismatch of these two materials.

To investigate the transport properties, the samples were cut into square pieces and Ohmic contacts were formed using In dots annealed at 350 °C.

Hall measurements at room temperature in the van der Pauw geometry have been performed for all samples. Values are summarized in Table I. For the samples in group A, the mobility was in the range from 1024 to 1481 cm^2/V s. All samples in group B grown under adaptive mode exhibited higher mobility, with a range from 1404 to 1904 cm^2/V s. The sample with the highest room temperature mobility, B2, exhibited a mobility of 2106 cm^2/V s at 80 K. This higher mobility at low temperature is consistent with previously published measurements of high quality InN.[27] Samples B1 and B3, which exhibited step-flow growth features, had comparable mobilities, 1404 and 1422 cm^2/V s, respectively, and average electron concentration around 3.2×10^{18} cm^{-3}.

It has been recently suggested that dislocation scattering is the primary mechanism limiting the electron mobility[28] of InN at room temperature. However, Thakur *et al.*[27] found that LO-phonon and deformation potential scattering dominate room temperature mobility for InN films with both low (5.6×10^{17}) and high (2.0×10^{20}) carrier densities. Our results summarized in Table I do not support the dominant role of dislocation scattering in electron mobility. The sample-to-sample differences in free carrier concentration do not appear to be related to screw or edge dislocation densities. Presumably, more experimentation and detailed temperature-dependent Hall measurements are needed to understand the relation between dislocations and InN mobility.

Raman spectra have been determined for all InN samples in this study. Figure 6 shows the results representative for sample B3 measured at 20 K and ambient temperature. The Raman spectra are dominated by the symmetry allowed E_2^2 and A_1(LO) phonons with energies corresponding to 493.0 and 584.6 cm^{-1} at room temperature.

Upon cooling to 20 K, the phonons blueshift by 1.9 cm^{-1} for E_2^2 and 4.9 cm^{-1} for A_1(LO). The E_2^2 phonon exhibits very narrow linewidth, ~4.2 cm^{-1} at ambient temperature, comparing well with previously published results[29,30] and indicative of high crystal quality.[31]

The E_2^2 phonon is commonly used in epitaxial films to determine stress induced by the substrate.[32,33] The stress-free Raman frequency of InN E_2^2 phonon and the corresponding Raman stress factor are reported to be 490.1 ± 0.2 cm^{-1} and -9.0 ± 0.8 cm^{-1}/GPa, respectively.[30] Using our x-ray measurements of in-plane strain ε_a along with the E_2^2 phonon shift and published elastic modulus of InN,[23] we obtain a Raman biaxial stress coefficient ($\Delta\omega/\Delta\sigma_a$) of -6.1 ± 0.9 cm^{-1}/GPa. This is somewhat smaller than the -9.0 ± 0.8 cm^{-1}/GPa value published for InN by Wang *et al.*,[30] but reasonably close to the reported values of -6.3 ± 1.4 cm^{-1}/GPa for AlN (Ref. 33) and -3.4 ± 0.3 cm^{-1}/GPa for GaN.[34] The A_1(LO) phonon linewidth observed in our spectrum is 11.4 cm^{-1}, agreeing well with prior reports of high crystal quality InN.[35] The presence of relatively intense A_1(LO) scattering in heavily doped InN has been reported by several authors[35,36] and attributed to a charge density fluctuation scattering mechanism at finite wave vector.[37] The relative intensity of A_1(LO) phonon to that of E_2^2 phonon is much lower in the current set of samples than those reported for InN with high free carrier concentration. The low intensity ratio seen in our data is consistent with relatively low free electron concentration, as determined by Hall measurements, and comparable to the similar ratio for both AlN (Ref. 33) and GaN (Ref. 38) with low free carrier densities.

For the same InN samples, room temperature (RT) photoluminescence has been measured, using an InGaAs detector and an Ar$^+$ laser at 514 nm with power intensity of 100 mW. The PL intensity is strong in each sample described here. The

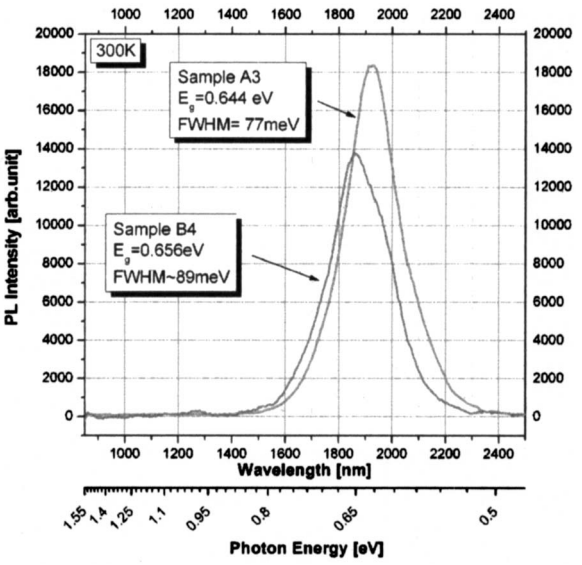

FIG. 7. Room temperature PL of InN.

samples in group A exhibit a single emission peak at energies between 0.635 and 0.658 eV. For the group B, the PL peaks are broader, suggesting a possible superposition of multiple PL peaks originating in layers with slightly different band edges. Typical PL spectra for the two groups are presented in Fig. 7. The band-edge PL is observed to shift systematically toward higher photon energy with increasing free carrier density. The measured shift is ~23 meV as the carrier concentration increases from 6×10^{17} to 4×10^{18} cm^{-3}. The shift observed in the band edge with free carrier density has been previously attributed to Moss-Burstein effect.[1,39]

IV. CONCLUSIONS

In conclusion, we have demonstrated the step-flow growth mode, with monolayer height terrace steps, using a production-style PA-MBE system, GEN200®. The surface morphology varies depending on the growth conditions. For the samples grown under 2D conditions throughout the cycle, step-flow features are observed on relatively large areas and rms roughness of 1.4 nm is obtained over an area of 5×5 μm^2. We have also observed the consequences of unintentional In droplets formation during the growth. We propose VLS as the growth mechanism under which the droplet formation impedes InN growth, when contrasted with neighboring regions, resulting in macroscopic defects in the epitaxial layer. The room temperature Hall mobility of InN layer, grown in such step-flow mode, is slightly higher than 1400 cm^2/V s, while for growth conditions yielding a smooth surface with no well-defined steps, mobility as high as 1904 cm^2/V s at room temperature which increases to 2106 cm^2/V s at 80 K has been obtained. Micro-Raman spectra show very narrow E_2^2 lines indicative of excellent InN crystalline quality. The samples exhibit intense PL emission at room temperature in the 0.64–0.66 eV range. The weak shift is consistent with free carrier concentration increase effects.

ACKNOWLEDGMENTS

Work at Texas Tech University was supported by the National Science Foundation (ECS-0609416) and the J. F. Maddox Foundation.

[1] J. Wu, W. Walukiewicz, W. Shan, K. M. Yu, J. W. Ager III, E. E. Haller, Hai Lu, and William J. Schaff, Phys. Rev. B **66**, 201403(R) (2002).
[2] Ashraful Ghani Bhuiyan, Kenichi Sugita, Ken Kasashima, Akihiro Hashimoto, Akio Yamamoto, and Valery Yu. Davydov, Appl. Phys. Lett. **83**, 4788 (2003).
[3] T. V. Shubina, S. V. Ivanov, V. N. Jmerik, D. D. Solnyshkov, V. A. Vekshin, P. S. Kop'ev, A. Vasson, J. Leymarie, A. Kavokin, H. Amano, K. Shimono, A. Kasic, and B. Monemar, Phys. Rev. Lett. **92**, 117407 (2004).
[4] V. Yu. Davydov *et al.*, Phys. Status Solidi B **229**, 787–795 (2002).
[5] J. Wu, W. Walukiewicz, K. M. Yu, J. W. Ager III, E. E. Haller, H. Lu, W. J. Schaff, Y. Saito, and Y. Nanishi, Appl. Phys. Lett. **80**, 3967 (2002).
[6] T. Matsuoka, H. Harima, and E. Kurimoto, Appl. Phys. Lett. **81**, 1246 (2002).
[7] J. Wu, W. Walukiewicz, K. M. Yu, W. Shan, J. W. Ager III, E. E. Haller, H. Lu, W. J. Schaff, W. K. Metzger, and S. Kurtz, J. Appl. Phys. **94**, 6477 (2003).
[8] C. Morioka, T. Yamaguchi, H. Naoi, T. Araki, A. Suzuki, and Y. Nanishi, Mater. Res. Soc. Symp. Proc. **798**, 760 (2003).
[9] R. Ascazubi, I. Wilke, K. Denniston, H. Lu, and W. J. Schaff, Appl. Phys. Lett. **84**, 4810 (2004).
[10] Y. Saito, H. Harima, E. Kurimoto, T. Yamaguci, N. Teraguci, A. Suzuki, T. Araki, and Y. Nanishi, Phys. Status Solidi B **234**, 796 (2002).
[11] S.-B. Che, T. Shinada, T. Mizuno, X. Wang, Y. Ishitani, and A. Yoshikawa, Jpn. J. Appl. Phys., Part 2 **45**, L1259 (2006).
[12] A. R. Smith, R. M. Feenstra, D. W. Greve, M.-S. Shin, M. Skowronski, J. Neugebauer, and J. E. Northrup, Appl. Phys. Lett. **72**, 2114 (1998).
[13] B. Heying, I. Smorchkova, C. Poblenz, C. Elsass, P. Fini, S. D. Baars, U. Mishra, and J. S. Speck, Appl. Phys. Lett. **77**, 2885 (2000).
[14] C. Adelmann, J. Brault, D. Jalabert, P. Gentile, H. Mariette, G. Mula, and B. Daudin, J. Appl. Phys. **91**, 9638 (2002).
[15] K. Xu and A. Yoshikawa, Appl. Phys. Lett. **83**, 251 (2003).
[16] W. K. Burton, N. Cabrera, and F. C. Frank, Philos. Trans. R. Soc. London, Ser. A **243A**, 299 (1951).
[17] X. Wang, S.-B. Che, Y. Ishitani, and A. Yoshikawa, Jpn. J. Appl. Phys., Part 1 **45**, L730–L733 (2006).
[18] G. Koblmuller, J. Brown, R. Averbeck, H. Riechert, P. Pongratz, and J. S. Speck, Appl. Phys. Lett. **86**, 041908 (2005).
[19] P. T. Dung and M. Láznička, Phys. Status Solidi A **97**, 103 (1986).
[20] P. F. Fewster and N. L. Andrew, J. Appl. Crystallogr. **28**, 451 (1995).
[21] V. Srikant, J. S. Speck, and D. R. Clarke, J. Appl. Phys. **82**, 4286 (1997).
[22] X. Wang, S.-B. Che, Y. Ishitani, and A. Yoshikawa, Appl. Phys. Lett. **90**, 151901 (2007).
[23] K. Wang and R. R. Reeber, Appl. Phys. Lett. **79**, 1602 (2001).
[24] H. Heinke, V. Kirchner, S. Einfeldt, and D. Hommel, Appl. Phys. Lett. **77**, 2145 (2000).
[25] V. M. Kaganer, O. Brandt, A. Trampert, and K. H. Ploog, Phys. Rev. B **72**, 045423 (2005).
[26] H. Heinke, V. Kirchner, S. Einfeldt, and D. Hommel, Phys. Status Solidi A **176**, 391 (1999).
[27] J. S. Thakur, R. Naik, V. M. Naik, D. Haddad, G. W. Auner, H. Lu, and W. J. Schaff, J. Appl. Phys. **99**, 023504 (2006).
[28] K. Wang, Y. Cao, J. Simon, J. Zhang, A. Mintairov, J. Merz, D. Hall, T. Kosel, and D. Jena, Appl. Phys. Lett. **89**, 162110 (2006).
[29] J. W. Pomeroy, M. Kuball, H. Lu, W. J. Schaff, X. Wang, and A. Yoshikawa, Appl. Phys. Lett. **86**, 223501 (2005).
[30] X. Q. Wang, S. B. Che, Y. Ishitani, and A. Yoshikawa, Appl. Phys. Lett. **89**, 171907 (2006).
[31] M. Giehler, M. Ramsteiner, P. Waltereit, O. Brandt, K. H. Ploog, and H. Obloh, J. Appl. Phys. **89**, 3634 (2001).
[32] M. Holtz, M. Seon, T. Prokofyeva, H. Temkin, R. Singh, F. P. Dabkowski, and T. D. Moustakas, Appl. Phys. Lett. **75**, 1757 (1999).
[33] T. Prokofyeva, M. Seon, J. Vanbuskirk, M. Holtz, S. A. Nikishin, N. N. Faleev, H. Temkin, and S. Zollner, Phys. Rev. B **63**, 125313 (2001).
[34] I. Ahmad, M. Holtz, N. N. Faleev, and H. Temkin, J. Appl. Phys. **95**,

1692 (2004).
[35]C. Pinquier, F. Demangeot, J. Frandon, J. C. Chervin, A. Polian, B. Couzinet, P. Munsch, O. Briot, S. Ruffenach, B. Gil, and B. Maleyre, Phys. Rev. B **73**, 115211 (2006).
[36]D. Y. Song, V. Kuryatkov, M. Basavaraj, D. Rosenbladt, S. A. Nikishin, M. Holtz, A. L. Syrkin, A. S. Usikov, V. A. Ivantsov, and V. A. Dmitriev, J. Appl. Phys. **99**, 111603 (2006).
[37]F. Demangeot, C. Pinquier, J. Frandon, M. Gaio, O. Briot, B. Maleyre, S. Ruffenach, and B. Gil, Phys. Rev. B **71**, 104305 (2005).
[38]A. S. Zubrilov, S. A. Nikishin, G. D. Kipshidze, V. V. Kuryatkov, H. Temkin, T. I. Prokofyeva, and M. Holtz, J. Appl. Phys. **91**, 1209 (2002).
[39]P. Carrier and S.-H. Wei, J. Appl. Phys. **97**, 033707 (2005).